

^{111}Cd from the ($^3\text{He}, 2n\gamma$) reaction and a rotational interpretation

Ning Wang,* F. A. Rickey, G. S. Samudra, P. C. Simms, and Sadek Zeghib†
 Tandem Accelerator Laboratory, Purdue University, Lafayette, Indiana 47907

(Received 27 July 1987)

The structure of ^{111}Cd was studied using the $^{110}\text{Pd}(^3\text{He}, 2n\gamma)^{111}\text{Cd}$ reaction, which populated a number of new nonyrast states. The experiments included γ -ray excitation functions, γ -ray angular distributions, and γ - γ coincidences. Even though ^{111}Cd is only two protons away from the closed $Z=50$ shell, there is evidence that it is slightly deformed. A symmetric particle-plus-rotor model has been used to interpret the results, and shows that rotational features are present.

I. INTRODUCTION

It has been demonstrated¹⁻⁴ that many features of transitional nuclei, particularly those in the mass-100 region, can be described by a standard symmetric particle-plus-rotor model if the Coriolis interaction is properly treated. These results have been used to argue that rotations are an important degree of freedom in regions previously thought to be vibrational, even though the deformations present are small. In the pursuit of this concept, it seems appropriate to ask how close to closed shells can nuclei exhibiting rotational phenomena be found.

A recent paper from this laboratory⁵ presented evidence that ^{111}Ag is clearly rotational, at $Z=47$. The 64 neutrons present have undoubtedly played a large role in influencing the deformation of ^{111}Ag . ^{111}Cd , with $Z=48$, is closer to the $Z=50$ closed shell, and is less deformed. The clearest indication of this is in the comparison of the ^{110}Pd and ^{110}Cd cores. In ^{110}Pd the energy of the first 2^+ state is 374 keV, while in ^{110}Cd it is 658 keV. Thus the study of ^{111}Cd and the interpretation of its observed structure seemed a logical step in the investigation of collective phenomena.

Previous studies of ^{111}Cd (Refs. 6-11) had established only states at low excitation energies or near the yrast line. ^3He induced reactions can populate a wider range of states. The present work has utilized the $^{110}\text{Pd}(^3\text{He}, 2n\gamma)^{111}\text{Cd}$ reaction to extend the knowledge of the structure of ^{111}Cd .

The observed structure was interpreted using a particle rotor model. In spite of the proximity to the $Z=50$ closed shell, ^{111}Cd exhibits the same kinds of rotational phenomena observed in more deformed nuclei.

II. EXPERIMENTAL TECHNIQUES

The measurements performed in this work included γ -ray excitation functions, angular distributions, and γ - γ coincidences. The target was a foil of isotopically enriched ^{110}Pd rolled to a uniform thickness of 5.1 mg/cm². The composition was 97.7% ^{110}Pd with the major impurity 1.3% ^{108}Pd . The two hyperpure Ge γ -ray detectors used in these experiments had energy resolutions of ~ 2.0 keV at 1332 keV and efficiencies of

$\sim 20\%$. The ^3He beam currents of 10 to 25 nA were supplied by the Purdue FN Tandem Van de Graaff accelerator.

The gain and zero level of the detector-electronics systems were monitored during a singles experiment using the Coulomb excitation lines from the gold beam-stop and lines from a ^{60}Co source placed near the detector. From the use of these internal standards, the energy of a relatively intense, clean γ -ray could be measured with an accuracy of approximately 100 eV. During the coincidence experiment the energy calibration was monitored by off-line measurements using a ^{182}Ta - ^{152}Eu radioactive source. There are about 65 strong lines ranging from 65 keV to 1408 keV whose energies have been determined previously to ± 0.1 keV.¹² The energy dependence of the efficiencies of the detectors was also measured with the same source, since the relative intensities of these lines have also been measured previously.¹²

On-demand beam pulsing was utilized in these measurements. Every time a γ -ray was detected the beam was deflected off the target until the γ -ray pulse had been processed. This technique reduced pileup, resulting in a 200% increase in the through-put rate of useful data and a reduction in background.

A. Excitation functions

Excitation functions were measured by accumulating γ -ray spectra at incident ^3He energies of 12, 13, 14, 15, 16, and 18 MeV. The measurement served two basic functions, selecting the appropriate beam energy for subsequent experiments, and providing spin information.

The competing reactions of concern were the ($^3\text{He}, 3n$) reaction and those involving proton emission. Relative probabilities of the latter reactions were found to increase with incident energy, and γ rays from them had been previously identified in the ^{111}Ag work. The relative probability of the $3n$ channel also increased with incident energy; thus an incident energy of 13 MeV was selected for subsequent experiments. A typical singles spectrum is shown in Fig. 1.

Excitation functions also provide valuable information about the spin of the state emitting the γ ray. The dominant effect on the shape of a particular excitation function is the energy dependence of the reaction. This was

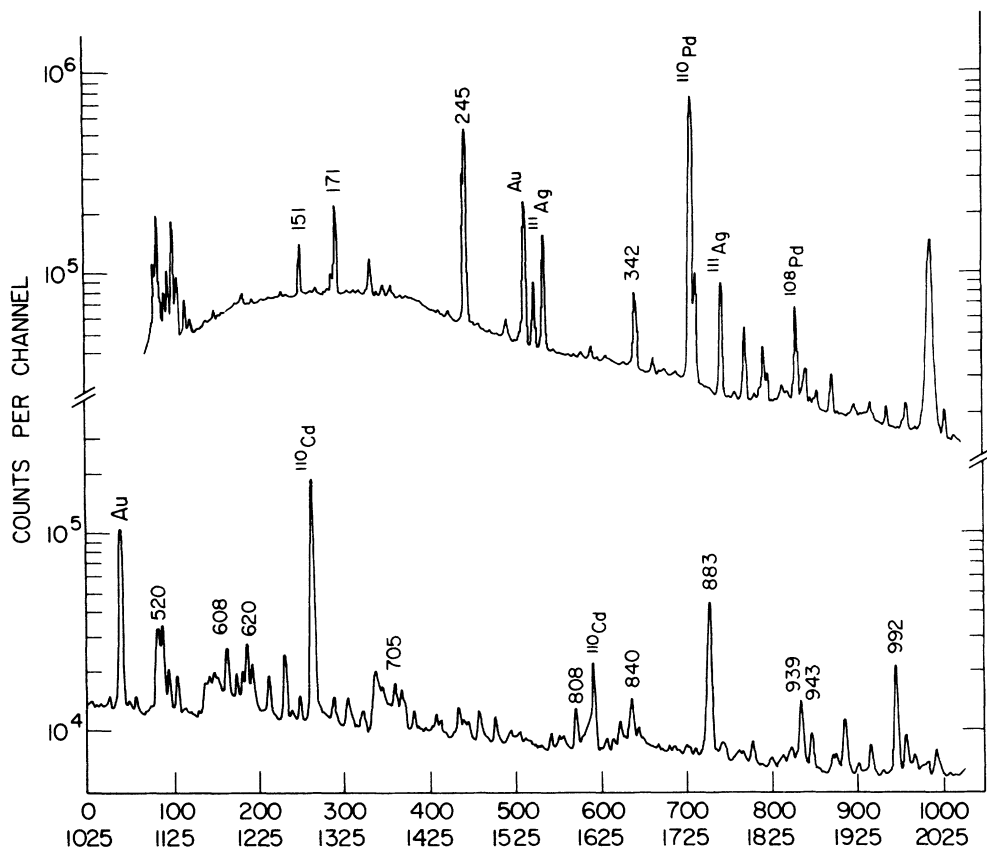


FIG. 1. Singles spectrum from the $^{110}\text{Pd}(^3\text{He},2n)^{111}\text{Cd}$ reaction at an incident energy of 13 MeV.

removed by normalizing all excitation functions to that of the 171.73-keV transition which depopulates the $\frac{7}{2}$ state at 416.60 keV in ^{111}Cd . It has been observed that the normalized excitation of each transition is then an exponential function of energy.¹³

$$I_{\gamma}(E) \approx e^{bE} \quad (1)$$

As the bombarding energy increases, so does the angular momentum carried into the system. Thus the population of higher spin states increases relative to lower spin states, which is reflected in the magnitude and signs of the exponential slope b in Eq. (1). These slopes are quite characteristic of the initial spin, and can be extracted by a linear least squares fit to the logs of the normalized intensities. The use of these slopes will be discussed later.

B. Angular distributions

The angular distribution measurement consisted of singles spectra collected at 0° , 23° , 45° , and 90° with respect to the beam axis. The alignment of the beam spot on the target with the axis of rotation of the detector was checked by placing a thin iron foil in the target position and bombarding it with 7 MeV protons. A small amount of radioactive ^{56}Co from the $^{56}\text{Fe}(p,n)^{56}\text{Co}$ reaction was thus produced at the beam position. Centering was then checked by counting the decay γ -radiation as a function of angle. The alignment of the

zero degree point of the table with the beam axis was checked by short measurements at $+90^\circ$ and -90° .

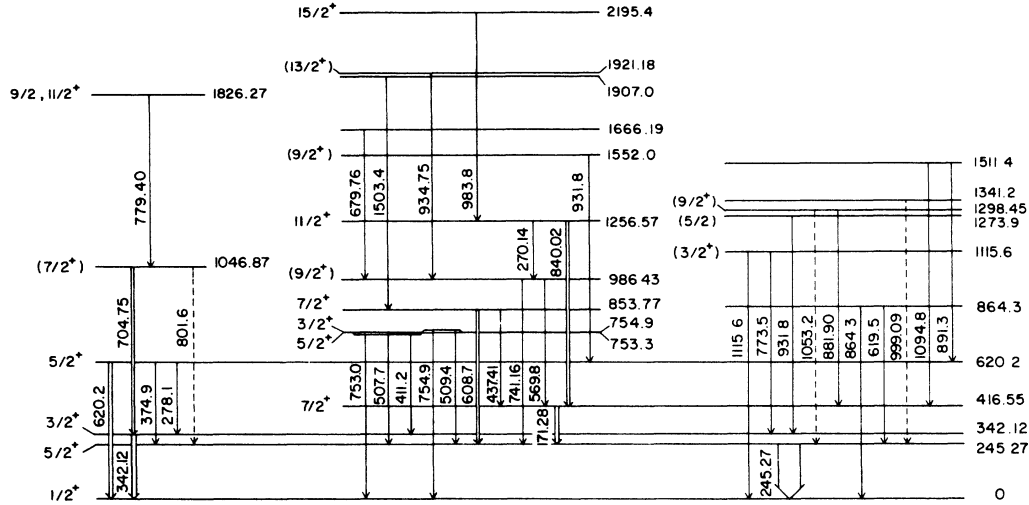
The standard angular distribution coefficients, A_{kk} , were extracted using a least-squares procedure. The theoretical angular distribution coefficients for maximum alignment, A_{kk}^0 , can be readily calculated as a function of the initial spin, the change in angular momentum, and the multipole nature of the transition.¹⁴ For the orientations obtained in ^3He induced reactions (at the incident energies of interest in the present work), all measured A_{44} values are expected to be zero within error. In general the knowledge of A_{22} alone does not result in unique spin assignments. Nevertheless A_{22} values used in conjunction with other observables can be useful, as will be discussed later.

C. γ - γ coincidence measurement

The coincidence measurement was performed using two detectors positioned at 0° and 100° with respect to the beam axis. Gamma coincidences were recorded event by event on magnetic tape. The data were then processed off-line, subtracting accidental coincidences. The procedures have been described previously.

III. THE LEVEL SCHEME

The level scheme deduced in the present work for ^{111}Cd is shown in Figs. 2 and 3. The level scheme con-

FIG. 2. The positive parity portion of the level scheme deduced for ^{111}Cd .

tains 30 states, 16 of which are new. The spin and parity assignments shown came from a combination of three sources: adopted values from Nuclear Data Sheets,¹⁵ our excitation function analysis, and our angular distribution measurements.

The excitation function analysis gave very consistent results. Table I lists slopes (and errors) for transitions depopulating states of known spins. The slopes for these reference transitions fall clearly into groups which are well separated. When the slopes for all transitions were compared to the ones shown in Table I, the same distinct groupings were observed. This leads to the adopt-

ed slope ranges for different spins given in the last column of the table. We believe that the slopes result in reliable spins assignments when a particular value lies unambiguously in one of the ranges.

Although the A_{44} values were not measurable due to the small nuclear orientation in these experiments, the angular distribution measurements still gave useful spin and parity information in some cases. If the measured A_{22} value is sufficiently large in magnitude, it can uniquely identify a mixed $\Delta I = \pm 1$ transition. By comparing measured A_{22} values for known $E2$ transitions to the theoretical A_{22}^0 values, one finds that attenuations are typically 0.2 to 0.5. Thus, for example, a measured A_{22} more negative than -0.4 corresponds to an A_{22}^0 of at least -0.8 .

$A_{22} < -0.4$ uniquely identifies a $\Delta I = \pm 1$ transition.

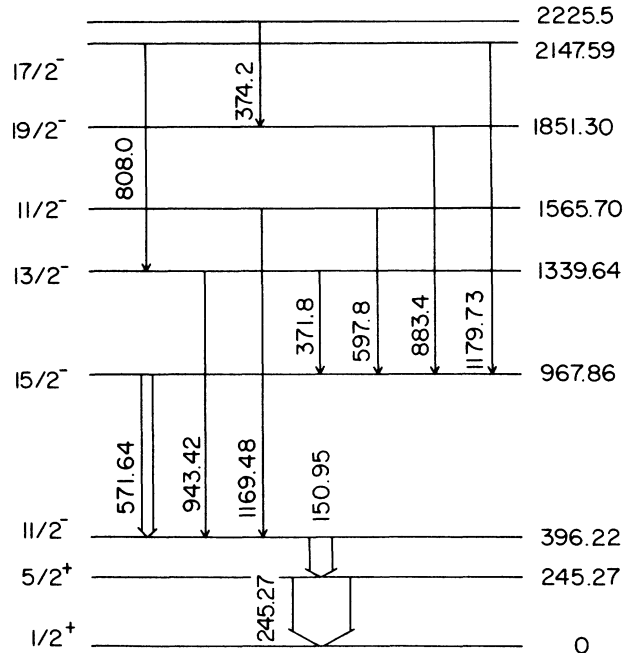
FIG. 3. The negative parity portion of the level scheme deduced for ^{111}Cd .

TABLE I. Reference slopes for excitation functions.

I_i	E_γ	Slope(Error) ($\times 1000$)	Adopted slope range ($\times 1000$)
$\frac{3}{2}$	342.12	-34(7)	-35(10)
	1115.6	-29(9)	
$\frac{5}{2}$	753.0	-22(2)	-15(10)
	410.9	-23(1)	
$\frac{7}{2}$	171.33	0(4)	0(10)
$\frac{9}{2}$	882.07	30(3)	25(15)
	150.95	50(10)	
$\frac{11}{2}$	839.97	57(10)	60(20)
	1169.48	56(26)	
$\frac{13}{2}$	943.42	104(17)	100(10)
$\frac{15}{2}$	571.64	125(12)	120(10)
	938.83	120(3)	

Similarly a large positive A_{22} specifies a $\Delta I = -1$ transition, except for small initial spins where $\Delta I = 0$ is possible. In addition the substantial mixing ratio associated with large A_{22} values means that the transition does not change parity. Small measured A_{22} values can also demand a mixed $E2-M1$ transition if the spin change is known from some other measurement. An A_{22} of the opposite sign expected for an unmixed transition clearly indicates mixing. However, a small A_{22} of the same sign indicates mixing if the orientation of the initial state is known and the A_{22} is smaller than expected for a pure dipole transition.

The level scheme with pertinent supporting information is also presented in Table II. The first and third columns give the state and transition energies. The energies given with two fractional digits are believed known to better than 0.1 keV, while those given with one fractional digit are believed known within 0.5 keV. In the second and fourth columns we give the initial and final spin if determined. The fifth column gives the energy of the final state. The placement of transitions in the level scheme was based not only on the existence of coincidences but consistency of intensities feeding and depopulating a proposed state. The presence of unresolved γ rays was determined by comparing coincidence and singles intensities. Column six of the table gives the measured intensities of transitions in ^{111}Cd , and column seven gives contaminant intensities and their sources where known. The adopted intensities are the relative A_{00} values from the angular distribution measurement for uncontaminated transitions or coincidence intensities for contaminated transitions. In column eight the A_{22} values from the angular distribution measurements are given, and in column nine the excitation function slopes are listed. Column ten contains labels which indicate the source of the spin and parity assignment. If Nuclear Data Sheets had given a spin assignment, the label "N" is used. An "N" alone indicates that we have nothing to add from our data. In many cases we have been able to remove ambiguities from previous assignments or assign spins to new states. The label "E" means that we have used this excitation function slope to support the spin assignment, and the labels "A" and "A π " indicate the use of our angular distribution to determine the spin and parity, respectively. Most of the assignments given are explained by these labels alone in a straightforward fashion. However, two spin assignments require specific discussion.

The 931.8-keV γ ray is a doublet. The large excitation function slope for the composite implies that one of the initial states has spin greater than or equal to $\frac{9}{2}$. The 1552.0-keV level is the best choice because it decays to a $\frac{5}{2}$ state, and has tentatively been assigned spin $\frac{9}{2}^+$. If this component of the doublet is an $E2$ transition, the other component must be a $\Delta I = 1$ transition to get an A_{22} near zero. Thus the 1273.9-keV state has tentatively been assigned spin $\frac{5}{2}$.

IV. DISCUSSION AND INTERPRETATION

The low-lying states of ^{111}Cd suggest that it is deformed. The $\frac{1}{2}^+$ ground state clearly has a substantial

$s_{1/2}$ component because of the large cross section in the (d,p) reaction.¹⁰ Likewise the first excited state, the $\frac{5}{2}^+$ state at 245 keV, must have a large $d_{5/2}$ component. This is evident from both the (d,p) cross section¹⁰ and its half-life.¹⁶ The 85 nsec half-life is too long for $s_{1/2}$ parentage and too short for $g_{7/2}$ parentage. The $\frac{7}{2}^+$ state at 417 keV must have a large $g_{7/2}$ component from its (d,p) cross section.¹⁰

It is difficult to obtain these energies and the correct spin sequence from the spherical shell model without substantial configuration mixing. However, the data can be understood readily if ^{111}Cd has a modest deformation.

Figure 4 shows the appropriate Nilsson diagram¹⁷ for neutrons in ^{111}Cd . At zero deformation there is a substantial energy separation of the $d_{5/2}$, $g_{7/2}$, and $s_{1/2}$ orbitals. As the deformation increases this separation obviously diminishes, and at a deformation of $\delta \sim 0.10$, Nilsson orbitals of all three parentages lie at similar energies. Thus in keeping with one of the goals of this work, we elected to perform a rotational calculation at a deformation of $\delta = 0.10$ in order to search for rotational phenomena in ^{111}Cd .

The details of the calculations have been described by Smith and Rickey¹⁸ and by Popli,¹⁹ and only a brief description will be presented here. The specific model utilizes a symmetric rotational Hamiltonian in the strong-coupling limit modified to include a variable moment-of-inertia (VMI).²⁰ The basis states are thus rotational states built on Nilsson single particle states, characterized by good K and Ω , the projection of the total angular momentum I and the particle angular momentum j on this symmetry axis, respectively. Pairing is treated in the BCS formalism. The Coriolis and recoil terms, which mix these states, are treated to all orders. This basic model has been used for years to interpret strongly deformed nuclei.

The parameters used in the calculation were constrained by systematics for the region and obvious features of the data. The VMI parameters $\mathcal{J}_0 = 0$ and $C = 0.06$ are typical for the region, as is the Coriolis attenuation of 0.8. The parameters κ and μ for the Nilsson calculation were dictated by feature of the data. A subset of the positive parity states, shown in the left side of Fig. 2, appear to be members of a $\frac{1}{2}^+$ rotational band from their energies and decay properties. This "band" must have a small decoupling parameter, which in this case governs the necessary separation of the $d_{1/2}$ and $d_{3/2}$ orbitals. The appropriate energies of the $d_{5/2}$ and $g_{7/2}$ orbitals relative to the $s_{1/2}$ orbital are suggested by the excitation energies of the lowest $\frac{5}{2}^+$ and $\frac{7}{2}^+$ states. These considerations result in the choices of $\kappa = 0.07$ and $\mu = 0.26$ or 0.34. For these parameters a Fermi energy of $\lambda = 46.5$ MeV was adopted, shown as a horizontal bar in Fig. 4, and $\Delta = 1.2$ MeV was taken from systematics.

In the comparison of the results of the calculation to the experimental results, emphasis has been placed on electromagnetic decay properties. Energies alone are not sufficient basis for comparison, since frequently there are several states of the same spin and parity which have similar excitation energies. The comparison of experi-

TABLE II. Analysis of γ rays emitted following the $^{110}\text{Pd}(^3\text{He}, 2n\gamma)^{111}\text{Cd}$ reaction at 13 MeV.

E_i	I_i	E_γ	I_f	E_f	^{111}Cd	Intensity		A_{22} ($\times 100$)	Ex. Funct. Slope ($\times 1000$)	I_π Sources
						Others				
Positive parity										
245.27	$\frac{5}{2}^+$	245.27	$\frac{1}{2}^+$	0.0	1000			-3(5)	-2(1)	N
342.12	$\frac{3}{2}^+$	342.12	$\frac{1}{2}^+$	0.0	183(3)			-2(4)	-34(7)	N
416.55	$\frac{7}{2}^+$	171.28	$\frac{5}{2}^+$	245.27	180(3)			5(5)	0(4)	N
620.2	$\frac{5}{2}^+$	620.2	$\frac{1}{2}^+$	0.0	90(15)	10(4) ^{110}Cd , 25(10)		7(4)	-31(14)	N
		374.9	$\frac{5}{2}^+$	245.27	22(4)	684(69) ^{110}Pd				
		278.1	$\frac{3}{2}^+$	342.12	5(3)	634(15) ^{197}Au				
		753.3	$\frac{5}{2}^+$	753.0	$\frac{1}{2}^+$	0.0	26(5)	13(5)	8(5)	-22(2)
754.9	$\frac{3}{2}^+$	411.2	$\frac{3}{2}^+$	342.12	22(5)			-18(8)	-23(1)	
		507.7	$\frac{5}{2}^+$	245.27	59(3)	1020(31) β^+				
		754.9	$\frac{1}{2}^+$	0.0	8(1)			9(8)	-69(22)	N,E
853.77	$\frac{7}{2}^+$	509.4	$\frac{5}{2}^+$	245.27	81(45)	1020(31) β^+				
		608.71	$\frac{5}{2}^+$	245.27	122(5)			-16(4)	8(1)	E,A
864.3		437.01	$\frac{7}{2}^+$	416.55	37(3)	9(3)		7(3)	-5(5)	E,A π
		864.8	$\frac{1}{2}^+$	0.0	11(2)					
986.43	$(\frac{9}{2}^+)$	619.5	$\frac{5}{2}^+$	245.27	4(2)	125(20)				
		741.16	$\frac{5}{2}^+$	245.27	39(2)					N
1046.87	$(\frac{7}{2}^+)$	569.8	$\frac{7}{2}^+$	416.55	107(10)	100(10)				
		704.75	$\frac{3}{2}^+$	342.12	102(10)			8(6)	0(1)	E
1115.6	$(\frac{3}{2}^+)$	801.6	$\frac{5}{2}^-$	245.27	10(8)					
		1115.6	$\frac{1}{2}^+$	0.0	40(10)	15(5)		-11(5)	-29(9)	N,A,E
		773.5	$\frac{3}{2}^+$	342.12	3(1)					
1256.57	$\frac{11}{2}^+$	840.02	$\frac{7}{2}^+$	416.55	107(4)			18(4)	57(10)	N,E
		270.14	$(\frac{9}{2}^+)$	986.43	6(1)			3(14)	83(40)	E
1273.9	$(\frac{5}{2}^+)$	931.8	$\frac{3}{2}^+$	242.12	15(3)	15(3) ^{111}Cd		-4(9)	80(40)	
1298.45	$(\frac{9}{2}^+)$	881.90	$\frac{7}{2}^+$	416.55	24(3)			17(9)	30(3)	E,A π
		1053.2	$\frac{5}{2}^+$	245.27	20(10)	6(2) ^{111}Cd , 22(3) ^{111}Ag				
1341.2		999.09	$\frac{3}{2}^+$	342.12	11(3)					
1511.4		891.3	$\frac{5}{2}^+$	620.2	18(5)			8(12)	-28(18)	
		1094.8	$\frac{7}{2}^+$	416.55	7(2)			34(28)	-4(48)	
1552.0	$(\frac{9}{2}^+)$	931.8	$\frac{5}{2}^+$	620.2	15(3)	15(3) ^{111}Cd		-4(9)	80(40)	E
1666.19		679.76	$(\frac{9}{2}^+)$	986.43	14(1)			-7(7)	35(58)	
1826.27	$\frac{9}{2}, \frac{11}{2}^+$	779.40	$(\frac{7}{2}^+)$	1046.87	11(1)			-4(13)	44(23)	E
1907.0		1053.4	$\frac{7}{2}^+$	853.77	6(2)	20(10) ^{111}Cd , 22(3) ^{111}Ag				
1921.18	$(\frac{13}{2}^+)$	934.75	$(\frac{9}{2}^+)$	986.3	23(3)					N
2195.4	$\frac{15}{2}^+$	938.8	$\frac{11}{2}^+$	1256.57	10(3)			33(10)	120(30)	N,E
Negative parity										
396.22	$\frac{11}{2}^-$	150.95	$\frac{5}{2}^+$	245.27	71(5)			-6(12)	50(10)	N
967.86	$\frac{15}{2}^-$	571.64	$\frac{11}{2}^-$	396.22	170(10)	20(10)		22(4)	125(12)	N,E
1339.64	$\frac{13}{2}^-$	943.42	$\frac{11}{2}^-$	396.22	56(2)	9(2) ^{111}Ag		6(5)	104(17)	N,E
		371.8	$\frac{15}{2}^-$	967.86	13(7)					
1565.70	$\frac{11}{2}^-$	1169.48	$\frac{11}{2}^-$	396.22	18(4)			10(31)	56(26)	N,E
		597.8	$\frac{15}{2}^-$	967.86	8(4)	41(7)		23(7)	62(18)	
1851.3	$\frac{19}{2}^-$	883.4	$\frac{15}{2}^-$	967.86	24(4)	483(11) ^{110}Cd				N
2147.59	$\frac{17}{2}^-$	808.0	$\frac{13}{2}^-$	1339.64	4(1)	63(3) ^{111}Ag				
		1179.73	$\frac{15}{2}^-$	967.86	12(1)			0(16)	152(44)	N,E
2225.5		374.2	$\frac{19}{2}^-$	1851.3	10(3)	674(70) ^{110}Pd				

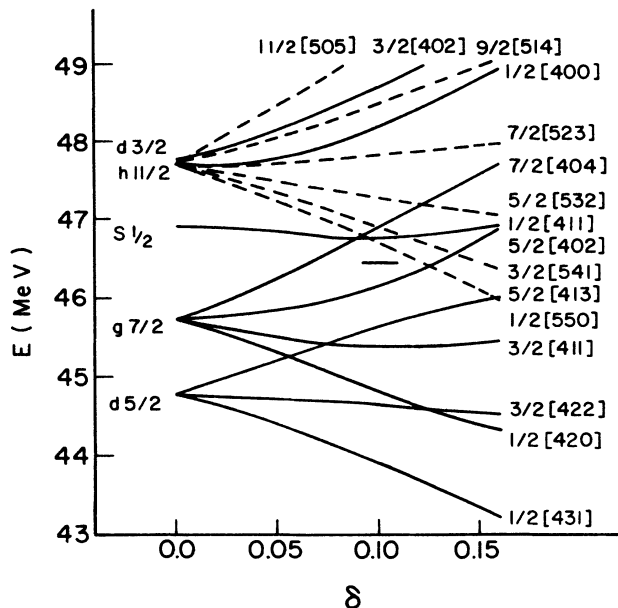


FIG. 4. Nilsson diagram for odd neutrons in ^{111}Cd . The horizontal bar indicates the approximate position of the Fermi surface.

mental and calculated branching ratios provides a more reliable identification.

Table III presents the comparison of experimental and calculated results for ^{111}Cd . This table includes only the experimental states which have been identified on the basis of their spins, energies, and branching ratios as

corresponding to rotational states predicted by this model. In general the calculation does an excellent job of reproducing the experimental features of ^{111}Cd . Most of the states observed (all of them at low excitation energies) have reasonable theoretical counterparts. Columns 1 and 2 give the experimental and theoretical initial energies for each state, and column 3 gives the initial spin. The model identification of the initial state is given in column 8. In the calculation we considered decay probabilities to all final states to which transitions were possible on the basis of energies and spin changes. However, the table only includes branches which were either observed or predicted to be observable. The fact that an unobserved but "allowed" branch was predicted to be statistically zero is a significant element of the identification, but if all of these possibilities were included the table would be uncomfortably large. For the branches included, column 4 gives the final spin and column 5 the γ -ray energy rounded to the nearest keV. Columns 6 and 7 give the experimental and theoretical branching ratios, and column 9 gives the model identification for each final state. This model identification reflects the basic character of the calculated wave function.

If the Coriolis mixing is small, a final state is dominated by a single Nilsson component. While this is generally true only for large deformations, it can also be the case at small deformations if the average value of j is small. The model prediction is then essentially a rotational band. The group of states identified in Table III as members of the $\frac{1}{2}^+[411]$ "band" fall in this category.

TABLE III. Comparison of experimental and calculated results for ^{111}Cd .

E_i (keV)		I_i^π	I_f^π	E_γ (keV)	Branching ratio		Theoretical Identification	
Expt	Theor				Expt	Theor	Initial State	Final State
0.0	0	$\frac{1}{2}^+$					$\frac{1}{2}^+[411]$	
245.27	250	$\frac{5}{2}^+$	$\frac{1}{2}^+$	245	1.0	1.0	$d_{5/2}, R=0$	$\frac{1}{2}^+[411]$
342.12	374	$\frac{3}{2}^+$	$\frac{1}{2}^+$	342	1.0	1.0	$\frac{1}{2}^+[411]$	$\frac{1}{2}^+[411]$
396.22	396	$\frac{11}{2}^-$	$\frac{5}{2}^+$	151	1.0	1.0	$h_{11/2}, R=0$	$d_{5/2}, R=0$
416.55	415	$\frac{7}{2}^+$	$\frac{5}{2}^+$	171	1.0	1.0	$g_{7/2}, R=0$	$d_{5/2}, R=0$
620.2	636	$\frac{5}{2}^+$	$\frac{1}{2}^+$	620	0.76	0.29	$\frac{1}{2}^+[411]$	$\frac{1}{2}^+[411]$
			$\frac{3}{2}^+$	375	0.19	0.59		$d_{5/2}, R=0$
			$\frac{5}{2}^+$	278	0.05	0.12		$\frac{1}{2}^+[411]$
			$\frac{7}{2}^+$	278	0.05	0.12		$\frac{1}{2}^+[411]$
753.3	767	$\frac{5}{2}^+$	$\frac{1}{2}^+$	753	0.25	0.13	$g_{7/2}, R=2$	$\frac{1}{2}^+[411]$
			$\frac{3}{2}^+$	508	0.50	0.70		$d_{5/2}, R=0$
			$\frac{5}{2}^+$	411	0.25	0.14		$\frac{1}{2}^+[411]$
			$\frac{7}{2}^+$	411	0.25	0.14		$\frac{1}{2}^+[411]$
754.9	791	$\frac{3}{2}^+$	$\frac{1}{2}^+$	755	0.31	0.42	$g_{7/2}, R=2$	$\frac{1}{2}^+[411]$
			$\frac{3}{2}^+$	509	0.57	0.53		$d_{5/2}, R=0$
			$\frac{5}{2}^+$	413	0.12	0.05		$\frac{1}{2}^+[411]$
			$\frac{7}{2}^+$	338	<0.06	0.001		$g_{7/2}, R=0$
853.77	864	$\frac{7}{2}^+$	$\frac{5}{2}^+$	608	0.77	0.85	$g_{7/2}, R=2$	$d_{5/2}, R=0$
			$\frac{3}{2}^+$	511	<0.03	0.00		$\frac{1}{2}^+[411]$
			$\frac{7}{2}^+$	437	0.23	0.14		$g_{7/2}, R=0$
			$\frac{5}{2}^+$	233	<0.03	0.02		$\frac{1}{2}^+[411]$
864.3	1106	$\frac{3}{2}^+$	$\frac{1}{2}^+$	864	0.35	0.35	$d_{3/2}, R=2$	$\frac{1}{2}^+[411]$
			$\frac{5}{2}^+$	620	0.65	0.65		$d_{5/2}, R=0$
967.86	1028	$\frac{15}{2}^-$	$\frac{11}{2}^-$	572	1.0	1.0	$h_{11/2}, R=2$	$h_{11/2}, R=0$

TABLE III. (Continued).

Expt	E_i (keV)	I_i^π	I_f^π	E_γ (keV)	Branching ratio		Theoretical Identification	
					Expt	Theor	Initial State	Final State
986.43	900	$\frac{9}{2}^+$	$\frac{5}{2}^+$	741	0.38	0.33	$g_{7/2}, R=2$	$d_{5/2}, R=0$
			$\frac{7}{2}^+$	570	0.62	0.66		$g_{7/2}, R=0$
1046.87	1243	$\frac{7}{2}^+$	$\frac{5}{2}^+$	802	0.09	0.01	$\frac{1}{2}^+[411]$	$d_{5/2}, R=0$
			$\frac{3}{2}^+$	705	0.91	0.77		$\frac{1}{2}^+[411]$
			$\frac{7}{2}^+$	630	<0.04	0.09		$g_{7/2}, R=0$
			$\frac{5}{2}^+$	427	<0.10	0.13		$\frac{1}{2}^+[411]$
1115.6	1352	$\frac{3}{2}^+$	$\frac{1}{2}^+$	1116	0.93	0.45	$d_{5/2}, R=2$	$\frac{1}{2}^+[411]$
			$\frac{5}{2}^+$	870	<0.12	0.28		$d_{5/2}, R=0$
			$\frac{3}{2}^+$	774	0.07	0.25		$\frac{1}{2}^+[411]$
1256.57	1169	$\frac{11}{2}^+$	$\frac{7}{2}^+$	840	0.95	0.99	$g_{7/2}, R=2$	$g_{7/2}, R=0$
			$\frac{9}{2}^+$	270	0.05	0.004		$g_{7/2}, R=2$
1273.9	1396	$\frac{5}{2}^+$	$\frac{3}{2}^+$	1028	<0.12	0.22	$d_{5/2}, R=2$	$d_{5/2}, R=0$
			$\frac{1}{2}^+$	931	1.0	0.75		$\frac{1}{2}^+[411]$
			$\frac{7}{2}^+$	857	<0.10	0.02		$g_{7/2}, R=0$
1298.45	1366	$\frac{9}{2}^+$	$\frac{5}{2}^+$	1053	0.45	0.35	$d_{5/2}, R=2$	$d_{5/2}, R=0$
			$\frac{7}{2}^+$	882	0.55	0.24		$g_{7/2}, R=0$
			$\frac{7}{2}^+$	446	<0.11	0.25		$g_{7/2}, R=2$
			$\frac{9}{2}^+$	312	<0.11	0.04		$g_{7/2}, R=2$
1339.64	1263	$\frac{13}{2}^-$	$\frac{11}{2}^-$	943	0.81	0.83	$h_{11/2}, R=2$	$h_{11/2}, R=0$
			$\frac{15}{2}^-$	372	0.19	0.17		$h_{11/2}, R=2$
1552.0	1787	$\frac{9}{2}^+$	$\frac{7}{2}^+$	1135	<0.33	0.05	$g_{9/2}, R=4$	$g_{7/2}, R=0$
			$\frac{5}{2}^+$	932	1.0	0.73		$\frac{1}{2}^+[411]$
			$\frac{7}{2}^+$	698	<0.33	0.15		$d_{3/2}, R=2$
1565.70	1593	$\frac{11}{2}^-$	$\frac{11}{2}^-$	1169	0.69	0.67	$h_{11/2}, R=2$	$h_{11/2}, R=0$
			$\frac{15}{2}^-$	598	0.31	0.00		$h_{11/2}, R=2$
			$\frac{13}{2}^-$	226	<0.19	0.14		$h_{11/2}, R=2$
1826.77	1864	$\frac{9}{2}^+$	$\frac{5}{2}^+$	1307	<0.10	0.06	$\frac{1}{2}^+[411]$	$d_{5/2}, R=0$
			$\frac{7}{2}^+$	1135	<0.33	0.05		$g_{7/2}, R=0$
			$\frac{5}{2}^+$	932	1.00	0.73		$\frac{1}{2}^+[411]$
			$\frac{7}{2}^+$	698	<0.33	0.15		$g_{7/2}, R=2$
1851.3	2015	$\frac{19}{2}^-$	$\frac{15}{2}^-$	883	1.0	1.0	$h_{11/2}, R=4$	$h_{11/2}, R=2$
1907.0	1968	$\frac{11}{2}^+$	$\frac{7}{2}^+$	1053	1.0	0.66	$g_{7/2}, R=4$	$g_{7/2}, R=2$
			$\frac{9}{2}^+$	931	<0.33	0.34		$g_{7/2}, R=2$
1921.18	1920	$\frac{13}{2}^+$	$\frac{9}{2}^+$	935	1.0	0.88	$g_{7/2}, R=4$	$g_{7/2}, R=2$
			$\frac{11}{2}^+$	665	<0.22	0.12		$g_{7/2}, R=2$
2147.59	2182	$\frac{17}{2}^-$	$\frac{15}{2}^-$	1180	0.75	0.79	$h_{11/2}, R=4$	$h_{11/2}, R=2$
			$\frac{13}{2}^-$	808	0.25	0.13		$h_{11/2}, R=2$
			$\frac{19}{2}^-$	296	<0.31	0.09		$h_{11/2}, R=4$
2195.40	2388	$\frac{15}{2}^+$	$\frac{11}{2}^+$	938	1.0	1.0	$g_{7/2}, R=4$	$g_{7/2}, R=2$

It should be pointed out that the dominant j components of members of this band alternate between $j=\frac{1}{2}$ and $j=\frac{3}{2}$ in the $I=\frac{1}{2}, \frac{3}{2}, \frac{5}{2}, \dots$ states, which is consistent with the large (d,p) cross sections for the $\frac{1}{2}^+$ and $\frac{3}{2}^+$ states.

When the Coriolis interaction has large effects, the final states of the calculation normally contain a dominant R and j rather than a dominant Ω . A group of states with the same R and j would have a spin I in the range $|R-j| \leq I \leq R+j$, and the number of states would be given by $2j+1$ ($R > j$) or $2R+1$ ($R < j$). The

average excitation energy of one of these groups increases with R as expected from the core. Thus the prediction of the rotational model resembles particle-core multiplets rather than bands. In ^{111}Cd this is the case for final states of $d_{5/2}, g_{7/2}$, and $h_{11/2}$ parentage.

The complete $g_{7/2}, R=2$ multiplet has been identified, as well as the $\frac{9}{2}^+$ through $\frac{15}{2}^+$ numbers of the $g_{7/2}, R=4$ multiplet. These states are so identified in Table III and grouped in the center portion of Fig. 2. The excellent agreement between the predicted and observed $g_{7/2}, R=2$ multiplet is a significant signature of rotation-

al phenomena in ^{111}Cd , since both yrast and non-yrast states are involved.

The experimental data for $d_{5/2}$ and $h_{11/2}$ multiplets are less complete. Thus the case for rotational behavior is less compelling. Nevertheless, the observations are consistent with the rotational predictions. Candidates for the $\frac{3}{2}^+$, $\frac{5}{2}^+$, and $\frac{9}{2}^+$ members of the $d_{5/2}, R=2$ multiplet have been identified. The "missing" members of this multiplet are predicted to lie at higher excitation energies. Only the near-yrast members of the $h_{11/2}, R=2$ and $R=4$ multiplets have been identified. Here the problem is the lack of experimental data on negative parity states due to the 48.6 minute half-life of the lowest $\frac{11}{2}^-$ state. All of the observed negative parity states are described quite well by the model.

An interesting isolated result of the calculation is that it predicts the half-life of the lowest $\frac{5}{2}^+$ state to be 69 nsec, in excellent agreement with the measured value of 85.0 nsec.

V. CONCLUSIONS

The ($^3\text{He}, 2n\gamma$) reaction successfully populated a number of new non-yrast states in ^{111}Cd . A symmetric particle plus rotor model has been used to interpret the level schemes deduced, and rotational phenomena have clearly been identified. A rotational band based on the $\frac{1}{2}^+$ ground state has been established up to spin $\frac{9}{2}^+$, and rotational "multiplets" of $g_{7/2}$, $d_{5/2}$, and $h_{11/2}$ parentage have been identified.

Because ^{111}Cd is only two protons away from the $Z=50$ closed shell, its deformation is small. Nevertheless the features expected for a slightly deformed rotor persist, and follow the patterns seen in other transitional nuclei in the region, with only a change in the inertial parameters required.

This work was supported in part by the National Science Foundation.

*Present address: Schlumberger Well Services, Houston, TX 77252.

†Present address: 3, Rue said Benkelouas, Constantine, Algeria.

¹C.S. Whisnant, K.D. Carnes, R.H. Castain, F.A. Rickey, G.S. Samudra, and P.C. Simms, Phys. Rev. C **34**, 443 (1986).

²Sadek Zeghib, F.A. Rickey, and P.C. Simms, Phys. Rev. C **34**, 1451 (1986).

³P.C. Simms, F.A. Rickey, and R.K. Popli, Nucl. Phys. **A347**, 205 (1980).

⁴K.D. Carnes, F.A. Rickey, G.S. Samudra, and P.C. Simms, Phys. Rev. C **35**, 525 (1987).

⁵Sadek Zeghib, F.A. Rickey, G.S. Samudra, P.C. Simms, and Ning Wang, Phys. Rev. C **36**, 939 (1987).

⁶S. Ohya, Y. Shida, O. Hashimoto, N. Yoshikawa, and M. Ishii, Nucl. Phys. **A325**, 408 (1979).

⁷K.P. Singh, D.C. Taya, Gulzar Singh, and H.S. Hans, Phys. Rev. C **31**, 79 (1985).

⁸T. Nagarjan, M. Ravindranath, and K.V. Reddy, Phys. Rev. C **3**, 254 (1971).

⁹T. Kracikova, I. Prochazka, Z. Hons, M. Fiser, and A. Kuklik, Czech. J. Phys. **B 27**, 1099 (1977).

¹⁰B. Rosner, Phys. Rev. **136**, B664 (1964).

¹¹J. McDonald and D. Porter, Nucl. Phys. **A109**, 529 (1968).

¹²R.A. Meyer, Lawrence Livermore Laboratory, Livermore, Calif., Report UCRL M-100 (1978).

¹³G. Kajrys, R. LeComte, S. Landsberger, and S. Manaro, Phys. Rev. C **28**, 1504 (1983).

¹⁴T. Yamazaki, Nucl. Data **A3**, 1 (1967).

¹⁵B. Harmatz, Nucl. Data Sheets **27**, 453 (1979).

¹⁶P.C. Simms and R.M. Steffen, Phys. Rev. **108**, 1459 (1957).

¹⁷S.G. Nilsson, K. Dan. Vidensk. Selsk. Mat.-Fys. Medd. **29**, No. 16 (1955).

¹⁸H.A. Smith, Jr. and F.A. Rickey, Phys. Rev. C **14**, 1946 (1976).

¹⁹Rakesh Popli, J.A. Grau, S.I. Popik, L.E. Samuelson, F.A. Rickey, and P.C. Simms, Phys. Rev. C **20**, 1350 (1979).

²⁰M.A.J. Mariscotti, G. Scharff-Goldhaber, and B. Buck, Phys. Rev. **178**, 1864 (1969).